LASER INTERFEROMETER GRAVITATIONAL WAVE OBSERVATORY
- LIGO -
CALIFORNIA INSTITUTE OF TECHNOLOGY
MASSACHUSETTS INSTITUTE OF TECHNOLOGY

Technical Note **LIGO-T2500248-v1** 08/27/2025

2025 LIGO SURF Final Report: Mapping and Correcting the Surface of the GQuEST End Mirrors

Rafael C. Volkamer-Pastor
Mentors: Daniel Grass and Lee McCuller

California Institute of Technology
LIGO Project, MS 18-34
Pasadena, CA 91125
Phone (626) 395-2129
Fax (626) 304-9834
E-mail: info@ligo.caltech.edu

Massachusetts Institute of Technology
LIGO Project, Room NW17-161
Cambridge, MA 02139
Phone (617) 253-4824
Fax (617) 253-7014
E-mail: info@ligo.mit.edu

LIGO Hanford Observatory
Route 10, Mile Marker 2
Richland, WA 99352
Phone (509) 372-8106
Fax (509) 372-8137
E-mail: info@ligo.caltech.edu

LIGO Livingston Observatory
19100 LIGO Lane
Livingston, LA 70754
Phone (225) 686-3100
Fax (225) 686-7189
E-mail: info@ligo.caltech.edu

http://www.ligo.caltech.edu/

Abstract

The GQuEST (Gravity from the Quantum Entanglement of Space-Time) end mirrors are susceptible to surface deformations which can cause incomplete interference at the differential output of the interferometer. I used an optical profiler to image the surface of these end mirrors and calculated the coupling coefficients to higher order Hermite-Gauss (HG) modes. A custom adjustable mirror mount was used to actuate on the end mirrors to decrease quadratic deformations in the mirror surface, and mitigate coupling to the HG_{02}, HG_{11}, and HG_{20} modes. The mount corrected 3.0×10^{-2} diopters of focusing power with a precision of 2.6×10^{-4} diopters, reducing the total mirror loss from $43,461$ ppm to 312 ppm. This enables GQuEST to lower the classical noise floor by minimizing the mirror thickness while minimally increasing the contrast defect. The benefit consists in a sufficiently low end mirror loss to confidently distinguish and measure (or bound) the quantum gravity fluctuations.

1 Introduction

The study of quantum gravity aims to find a joint theory of gravitation and quantum mechanics. Substantial theoretical efforts have been made toward quantum gravity. Erik Verlinde and Kathryn Zurek predict 'geontropic' fluctuations, stochastic fluctuations of space-time geometry induced by entropy [1]. GQuEST (Gravity from the Quantum Entanglement of Space-Time), an experiment in the McCuller Lab at Caltech, aims to test this theory by analyzing the phase of light. When light propagates through a space with these fluctuations, it is predicted to accumulate a phase difference relative to light traveling without the fluctuations. The goal of GQuEST is to detect these geontropic fluctuations using a tabletop Michelson interferometer, refer to Figure 1.

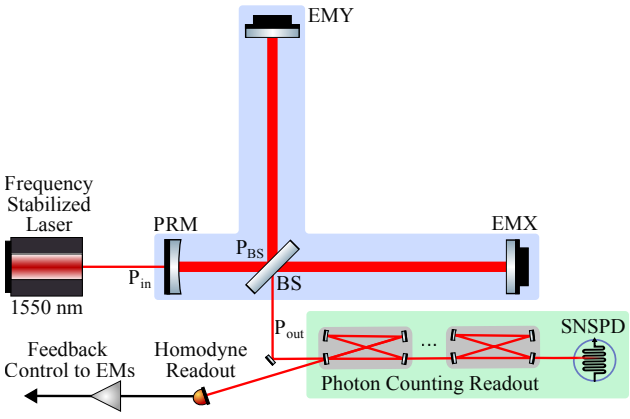

Figure 1: Michelson Interferometer used in GQuEST setup [2].

Geontropic fluctuations are characteristically of very low amplitude, roughly 7 orders of magnitude below the quantum shot noise of a lab scale, high power interferometer. Hence, to get strong results (5σ significance test), experiments are expected to take a run time of around 6 months [2]. Although feasible, this duration can be reduced by using the novel

photon-counting technique proposed by GQuEST. The method aims to filter the output light such that only photons carrying the signal are detected; however, some noise at the signal frequency will still pass. An advantage to this new method is that it is not limited by quantum shot noise, unlike the traditional homodyne readout of interferometers. This drastically reduces the total noise to 1 order of magnitude above the signal (compared to the previous 7), causing classical noise, for example vibrations in optical components, to become the new bottleneck. The photon counting method is expected to get strong results (5σ significance test) in weeks, compared to 6 months using a traditional homodyne readout [2].

2 Objective

This project focuses on the consequences of reducing classical noise for the GQuEST end mirrors and the resulting necessary modifications. The contribution to the noise floor from the substrate of the mirror can be approximated by the following analytical equation,

$$\bar{S}_L^{SMN}(\Omega) = \frac{16 k_B T h \varphi_s}{\pi^3 M_s w^2 \Omega} \tag{1}$$

where k_B is Boltzmann's constant, T is temperature, h is mirror thickness, φ_s is the mechanical loss angle of substrate, M_s is the P-wave modulus of substrate, w is beam width (2σ radius in intensity), and Ω is measurement angular frequency [2]. It is easier to modify the mirror thickness than the temperature of the interferometer to reduce noise. Hence, GQuEST plans to utilize 2 mm silicon mirrors, bringing the noise floor from the substrate below the coating thermal noise floor, which we have less control over.

However, minimizing the mirror thickness causes the mirror to be more pliable. The GQuEST mirrors are made out of a substrate with a highly reflective Bragg reflection coating, similar to LIGO's mirrors. When the coating is applied it curves the face of the mirror as described,

$$r_{curv} \approx \frac{E_s h^2}{6 \sigma_c h_c (1 - v_s)} \tag{2}$$

where E_s is Young's modulus of the substrate (the stiffness of the mirror), h is mirror thickness, σ_c is the coating stress, h_c is the thickness of the coating, and v_s is the Poisson ratio for substrate. With the current proposed parameters for GQuEST, $r_{curv} \approx 7.6$m [2]. Hence, it is clear that although minimizing the mirror thickness (h) is beneficial for reducing classical noise it results in a sharper mirror curve, the consequences of which I will further explain in the following paragraph.

When light reflects off of a curved mirror surface some of the light is bumped into higher-order modes (HOMs). If the mirrors are not curved identically the HOMs will not all

destructively interfere and hence produce a contrast defect, which causes extra light to escape the interferometer, increasing the 'bad' photon rate (photons passing the filter due to imperfections and not geontropic fluctuations). The focusing power into HOMs can be estimated to be roughly $D = 2/r_{curv}$. Specifically, a difference in the end-mirror curvature on the X and Y arms of the interferometer would scatter the majority of the light into the (Hermite-Gauss) HG_{20}, HG_{11}, and HG_{02} modes. The current hope is that these will be the only significant modes we need to correct for.

The amplitude coefficients of these modes would be

$$k_{nm} \approx \frac{kD_{nm}w^2}{4\sqrt{2}}; n + m = 2 \tag{3}$$

where D_{nm} is the focusing power into the specific HG_{nm} mode. This scattered light creates a contrast defect of $\Lambda_{CD} = k_{20}^2 + k_{11}^2 + k_{02}^2$. Therefore, to achieve a significantly low contrast defect ($\Lambda_{CD} < 50$ppm) total curvature mismatch needs to be $D_{tot} = \sqrt{D_{20}^2 + D_{11}^2 + D_{02}^2} < 3 \times 10^{-4}$ diopters. With the current proposed parameters for GQuEST the mirror mismatch is expected to be roughly 0.26 diopters, indicating that there will need to be some curvature correction method [2].

GQuEST will initially compensate by coating the back of the mirror with an anti-reflective coating of custom thickness to cancel as much of the induced curvature as possible. An additional approach is to try to match the curvature of the two end mirrors in hopes to cancel out the HOMs. However, it is likely we can't find perfect pairs and hence should not rely on their destructive interference. Instead, the remainder of the curvature difference will be adjusted through a custom mirror mount that is designed to twist and bend the mirror to counteract the curvature induced by the coating stress.

The goal of this project is to configure and test a custom adjustable mirror mount to correct the curved surface of the GQuEST end mirrors to enable the photon counting method as a tool to study quantum gravity. This work builds on a previous project by LIGO SURF student Erin McGee, who worked under the mentorship of Daniel Grass during the summer of 2024; the current project serves as a continuation of her efforts and was also mentored by Daniel Grass.

3 Approach

3.1 Mirror Surface and Deformations

The Zernike polynomials are an orthogonal basis on the unit disk. They serve as a useful tool to visualize the mirror deformations. The first 10 Zernike polynomials can be seen in figure 2.

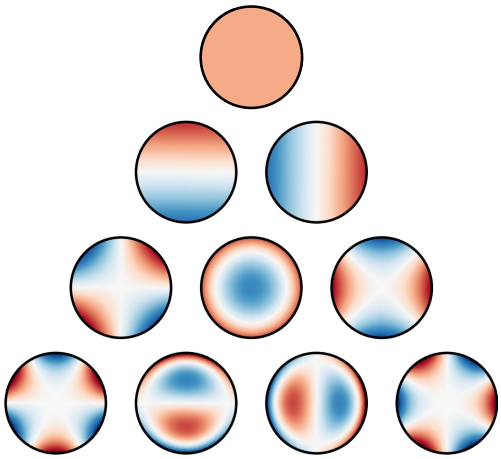

Figure 2: Visualization of the Zernike Polynomials made by Nschloe [3]. The Zernike polynomials provide an orthogonal basis on the unit disk. The 0th degree, top most mode, refers to a mirrors position on the optical axis. The 1st degree, two modes in the second row, refer to the tip and tilt of the mirror. This research is concerned with 2nd degree, third row, deformations, the +mode, Omode, and Xmode.

The 0th degree Zernike polynomial represents the position of the mirror along the optical axis. The 1st degree Zernike polynomials refer to the tip and tilt of the mirror. These three degrees of freedom can be corrected using a traditional kinematic mount. The next order of deformations are the +mode, Omode, and Xmode (read left to right in figure 2). These names have been chosen to resemble their equilibrium lines. The adjustable mirror mount is designed to bend the mirror in these 2nd degree modes.

This project uses a 4D NanoCam HD, a small scale optical profiler, as its primary measurement apparatus. The profiler can take surface measurements of the mirror to within an angstrom. This allows us to capture a height map of the mirror and observe how the mirror surface reacts to adjustments from the mount. From this data we are able to calculate couplings into higher order modes as well as total power loss.

3.2 Adjustable Mirror Mount

GQuEST uses spoked silicon mirrors. This research tests a circular barrel shape and an octagonal barrel shape. The spokes of the mirrors sit in 4 aluminum clamping Ts, figure 3a. These Ts are separately clamped to the larger mirror mount at their base. The adjustable mirror mount has 12 adjustment screws (figure 3) 4 screws on the front and 8 screws on the back.

The adjustment screws are able to push, pull, and twist the clamping Ts. This induces the +mode, Omode, and Xmode that we are aiming to correct. By using fine adjustment screws (250 μm/rev) we are able to correct nm scale deformations on the mirror surface. Demonstrations of this will be shown later in this report.

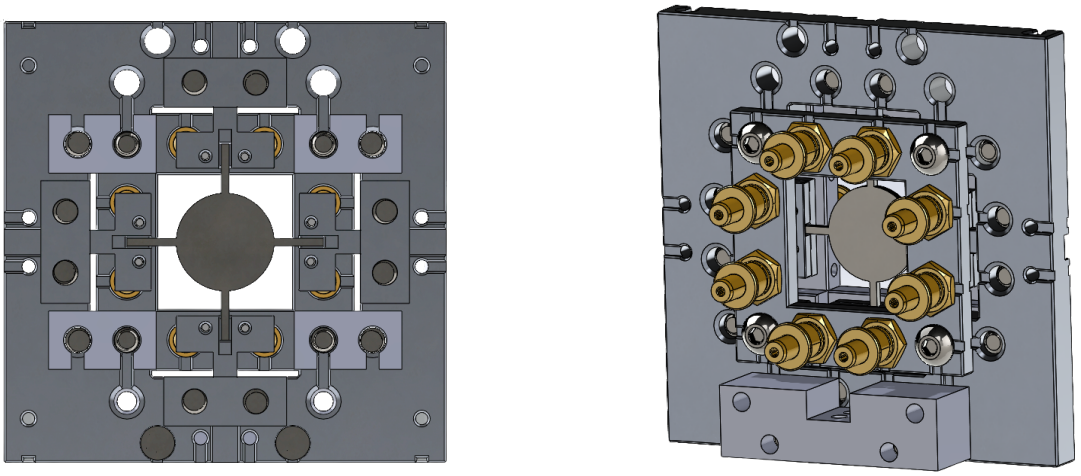

(a) Unclamped Mirror (b) Adjustment Screw

Figure 3: Image of the GQuEST Adjustable Mirror Mount. In the left image we can see the circular spoked mirror sitting in the mirror mount before it is clamped in place. The spokes of the mirror are being held by the clamping Ts. In the right image we see the final mirror once the adjustment screws are placed onto the mount. There are 4 additional adjustment screws on the other side of the mirror.

3.3 Coupling Coefficients

As a reminder, we are interested in how the mirror surface couples the incoming HG_{00}, gaussian, laser beam into higher order modes. I have developed a simulation in MATLAB which takes the height map of the mirror, as measured by the optical profiler, and calculates the coupling coefficients to higher order modes.

The code calculates these amplitude coefficients using the following two equations. This tells us how much of the incoming beam is contained in the outgoing beam,

$$k_{nmn'm'} = \iint u^*_{n'm'} e^{2ik\tilde{z}(x,y)} u_{nm}(x,y) dx dy \tag{4}$$

where k is the laser wave number, $\tilde{z}(x,y)$ is the displacement of the surface of the mirror, and u_{nm} is a function of the beam and the relevant modes given by

$$\begin{aligned} u_{nm}(x,y) = \left(\frac{1}{2^{n+m-1} n! m! \pi}\right)^{1/2} \left(\frac{1}{w_0}\right) \left(\frac{q_0}{q(z)}\right) \left(\frac{q_0 q^*(z)}{q^* q(z)}\right)^{(n+m)/2} \\ \cdot H_n\left(\frac{\sqrt{2}x}{w(z)}\right) H_m\left(\frac{\sqrt{2}y}{w(z)}\right) e^{-ik\frac{(x^2+y^2)}{2q(z)}} \end{aligned} \tag{5}$$

where n and m refer to the Hermite–Gaussian modes HG_{nm}, w_0 is beam waist, $w(z)$ is the beam width, q is the complex beam parameter, x and y are the transverse directions of the beam, z is the beam axis, and H is the Hermite Polynomial of corresponding order n or m [4]. As we assume an incoming HG_{00} mode, we set $n', m' = 0$. The bounds of the integral are set by the data bounds of $\tilde{z}(x, y)$. This simulation tells us how much power we loose to HOMs and is used to calculate k_{nm} in equation 3, allowing us to calculate the focusing power of the mirror.

3.4 Flattening Workflow

The following figure attempts to describe how the optical profiler, coupling coefficient code, and adjustable mirror mount all interact together.

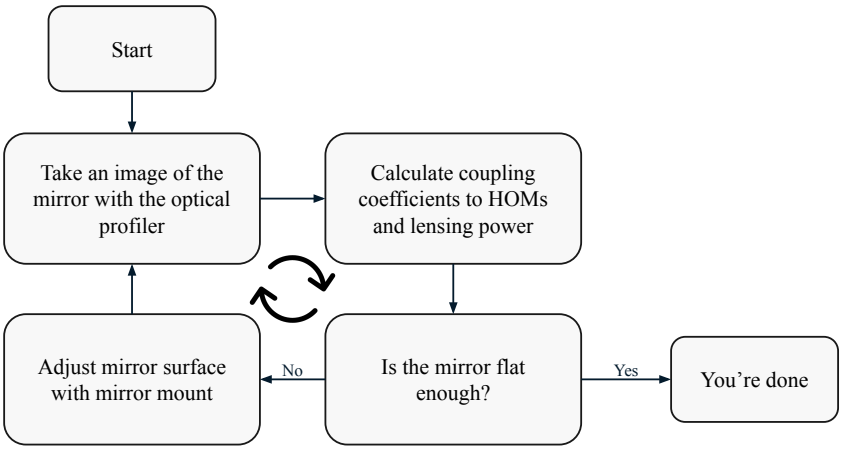

Figure 4: Diagram of Project Workflow. This is a flowchart of how the optical profiler, analysis code, and adjustable mirror mount work together. Dropping the focusing power by two orders of magnitude can be achieved in a day. This project defined "flat enough" when the rms of the mirror is under 1 nm.

4 Achievements

4.1 NanoCam Limitations

There is a major limitation with the NanoCam: with the current set of objectives we are only able to capture a 3.5 mm by 4 mm area. The 2σ power radius of the laser on the mirror is expected to be around 3 mm, which means the area the NanoCam images does not fully encompass the laser beam. Not only is there missing power, but additionally the Hermite Polynomials are not orthogonal on such a small scale. This means that the coupling coefficients calculated from the limited domain will not be perpendicular and will result in additional non-mirror related HOMs.

Additionally, we have found the 4D NanoCam has some astigmatism in its optical system, the root of which is unclear. The astigmatism adds an additional 5000ppm of loss to a flat mirror. This is 2 orders of magnitude above the goal loss for the end mirrors and will need to be corrected for. Furthermore, the lens of the NanoCam did not fit into the adjustable mirror mount. We switched one of the adjustment screws for a lower profile though coarser screw to better fit the geometry of the NanoCam. This allowed us to be able to take images of the mounted mirror.

4.1.1 Least Squares Fit and Extrapolation

The current approach is to use a combination of a least squares polynomial fit and the matrix approach to calculate our coupling coefficients. Simulations indicate that we require roughly a 10 mm × 10 mm image to get accurate coupling into HOMs. To expand our imaging area we construct a least squares fit for our 3.5 mm × 4 mm image and extrapolate it to the larger 10 mm × 10 mm domain. We chose to use a polynomial fit as the 2nd order deformations we are primarily concerned with are quadratic in nature. The +mode can be described as $z = xy$, the Omode can be described as $z = x^2 + y^2$, and the Xmode can be described as $z = x^2 - y^2$. Our model for the mirror surface is,

$$Z(x, y) = d + a(x - f)^2 + b(x - f)(y - g) + c(y - g)^2 + ... \text{ higher order polynomials,} \quad (6)$$

and we are able to omit the linear terms as we can correct for the tip and tilt using mounting stages. The piston term is included in our model to let the center (f, g) have an additional degree of freedom. We can fit the mirror surface up to a desired polynomial degree and evaluate the accuracy of the model using the R-squared value. We found that the majority of the mirror deformations were quadratic as expected.

The polynomial fit is good at picking up on larger deformations of the mirror surface, but would require an extremely high degree fit to pick up on surface roughness. To account for this we take the residuals of the least squares fit and calculate their scattered power. This is calculated using a formula developed by Robert Nyman and Benjamin Walker for scattering from surface roughness [5] (confirmed numerically),

$$P_s = 4k^2\sigma^2 \quad (7)$$

where P_s is the scattered power, k is the laser wave number, and σ is the weighted rms of the residuals. We use the Gaussian beam as our weighting function as we are aiming to quantify power loss. The total power loss is the sum of the scattered power and the power coupled into higher order modes,

$$P_{tot} = P_s + (1 - k_{00}^2). \quad (8)$$

To reiterate, k_{00} is calculated from the extrapolated polynomial fit and P_s is calculated from the residual roughness.

4.1.2 The Matrix Approach

The matrix approach aims to work around the inherit clipped domain of our height map by working in two Hermite Gauss bases. The first of which is the clipped HG basis, constructed from the coupling coefficients that we calculate from the restricted NanoCam domain. We will get some overlapping into different modes as the Hermite Polynomials are not orthogonal on this scale, more on how to resolve this briefly. The second basis is the full HG basis, which will be the coupling coefficients on an infinite domain. This is what we are ultimately interested in as it is the natural basis for HOMs which we are concerned about lensing into. We express the conversion between both bases as a matrix equation.

$$\begin{bmatrix} \mathrm{HG}_{\mathrm{clipped},1} \\ \mathrm{HG}_{\mathrm{clipped},2} \\ \vdots \\ \mathrm{HG}_{\mathrm{clipped},n} \end{bmatrix} = \begin{bmatrix} m_{11} & m_{12} & \cdots & m_{1m} \\ m_{21} & m_{22} & \cdots & m_{2m} \\ \vdots & \vdots & \ddots & \vdots \\ m_{n1} & m_{n2} & \cdots & m_{nm} \end{bmatrix} \cdot \begin{bmatrix} \mathrm{HG}_{\mathrm{full},1} \\ \mathrm{HG}_{\mathrm{full},2} \\ \vdots \\ \mathrm{HG}_{\mathrm{full},m} \end{bmatrix} \tag{9}$$

The indexing in equation 9 follows the subsequent pattern for $n + m \leq 3$.

Index	Hermite Gauss Mode
HG_1	HG_{00}
HG_2	HG_{10}
HG_3	HG_{01}
HG_4	HG_{20}
HG_5	HG_{11}
HG_6	HG_{02}
HG_7	HG_{30}
HG_8	HG_{21}
HG_9	HG_{12}
HG_{10}	HG_{03}

Table 1: Indexing for Hermite Gauss Modes. This table demonstrates the indexing pattern for the HG modes for $n + m \leq 3$.

To calculate the M matrix for equation 9, each m_{ij} is defined as the overlap integral of the HG_i and HG_j mode over the restricted NanoCam area. One can take the inverse of this matrix to convert from $\mathrm{HG}_{clipped}$ to HG_{full}. Note this sometimes requires a pseudoinverse. This matrix takes into account the non-orthonormality of the Hermite Polynomials on the smaller area by having non-zero non-diagonal entries. This matrix simplifies to the identity matrix as the NanoCam area becomes much greater than the beam spot size, and is used in conjunction with the least squares fit.

4.1.3 Correcting Inherit NanoCam Astigmatism

I found an inherit astigmatism with the NanoCam. I took two images, one of the unstressed unmounted mirror and the same mirror rotated clockwise 90°. I found that the mirrors looked nearly identical (they did not appear to be rotated). After taking multiple pictures I concluded that the NanoCam was adding an offset to the image.

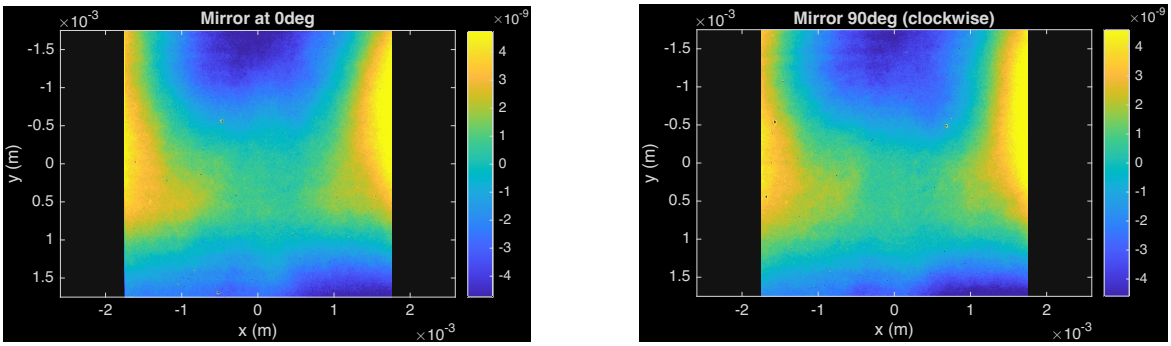

(a) Mirror 0° (b) Mirror −90°

Figure 5: Mirror Imaged Aligned and Rotated Clockwise 90°. These images show the offset due to the NanoCam. They should be rotated 90° from each other but they both seem to have the same saddle shape.

One technique to find and correct for this offset is to use a reference flat and subtract the resulting image from future data. We developed a secondary algebraic method to correct for the astigmatism that avoids using a reference flat. This method is described below.

Suppose we take our two height maps from figure 5. We can label the image captured of the aligned mirror Z_1 and the image of the 90° rotated mirror Z_2. These images are represented as matrices and are the combination of the mirror surface and the NanoCam offset.

$$Z_1 = m_1 + n \tag{10}$$
$$Z_2 = m_2 + n \tag{11}$$

Consider the matrix rotation operation $\hat{r}$ (note that this operation is distributive). Because all we did was rotate the mirror, we can say that $\hat{r}m_1 = m_2$. We can apply $\hat{r}^{-1}$ to the Z_2 equation and solve the system,

$$\hat{r}^{-1}Z_2 = \hat{r}^{-1}m_2 + \hat{r}^{-1}n \tag{12}$$
$$Z_1 - \hat{r}^{-1}Z_2 = m_1 + n - \hat{r}^{-1}m_2 - \hat{r}^{-1}n \tag{13}$$
$$Z_1 - \hat{r}^{-1}Z_2 = n - \hat{r}^{-1}n \tag{14}$$

We are curious to find the n matrix, as this represents the offset of the NanoCam, and we know Z_1 and Z_2. Note that we have eliminated the m_1 and m_2 terms. The resulting system can be solved using a matrix equation. As an example, suppose a smaller 3×3 case with $\hat{r}$ representing a rotation 90° clockwise.

$$n = \begin{bmatrix} n_{11} & n_{12} & n_{13} \\ n_{21} & n_{22} & n_{23} \\ n_{31} & n_{32} & n_{33} \end{bmatrix}, \quad \hat{r}^{-1}n = \begin{bmatrix} n_{13} & n_{23} & n_{33} \\ n_{12} & n_{22} & n_{32} \\ n_{11} & n_{21} & n_{31} \end{bmatrix} \tag{15}$$

$$n - \hat{r}^{-1}n = \begin{bmatrix} n_{11} - n_{13} & n_{12} - n_{23} & n_{13} - n_{33} \\ n_{21} - n_{12} & n_{22} - n_{22} & n_{23} - n_{32} \\ n_{31} - n_{11} & n_{32} - n_{21} & n_{33} - n_{31} \end{bmatrix} \tag{16}$$

This equation can be represented as a matrix operation if we reshape n into a column vector.

$$\begin{bmatrix} 1 & 0 & 0 & 0 & 0 & 0 & -1 & 0 & 0 \\ 0 & 1 & 0 & -1 & 0 & 0 & 0 & 0 & 0 \\ -1 & 0 & 1 & 0 & 0 & 0 & 0 & 0 & 0 \\ 0 & 0 & 0 & 1 & 0 & 0 & 0 & -1 & 0 \\ 0 & 0 & 0 & 0 & 0 & 0 & 0 & 0 & 0 \\ 0 & -1 & 0 & 0 & 0 & 1 & 0 & 0 & 0 \\ 0 & 0 & 0 & 0 & 0 & 0 & 1 & 0 & -1 \\ 0 & 0 & 0 & 0 & 0 & -1 & 0 & 1 & 0 \\ 0 & 0 & -1 & 0 & 0 & 0 & 0 & 0 & 1 \end{bmatrix} \begin{bmatrix} n_{11} \\ n_{21} \\ n_{31} \\ n_{12} \\ n_{22} \\ n_{32} \\ n_{13} \\ n_{23} \\ n_{33} \end{bmatrix} \tag{17}$$

Hence, if we define $\vec{Z}$ to be the column vector representation of $Z_1 - \hat{r}^{-1}Z_2$ and $\vec{n}$ to be the column vector representation of n, then we can solve for $\vec{n}$,

$$\vec{Z} = \begin{bmatrix} 1 & 0 & 0 & 0 & 0 & 0 & -1 & 0 & 0 \\ 0 & 1 & 0 & -1 & 0 & 0 & 0 & 0 & 0 \\ -1 & 0 & 1 & 0 & 0 & 0 & 0 & 0 & 0 \\ 0 & 0 & 0 & 1 & 0 & 0 & 0 & -1 & 0 \\ 0 & 0 & 0 & 0 & 0 & 0 & 0 & 0 & 0 \\ 0 & -1 & 0 & 0 & 0 & 1 & 0 & 0 & 0 \\ 0 & 0 & 0 & 0 & 0 & 0 & 1 & 0 & -1 \\ 0 & 0 & 0 & 0 & 0 & -1 & 0 & 1 & 0 \\ 0 & 0 & -1 & 0 & 0 & 0 & 0 & 0 & 1 \end{bmatrix} \vec{n} \tag{18}$$

From $\vec{n}$ we can reconstruct n. By using sparse matrices we make it simple for a computer to solve and reconstruct. The results of this approach for figure 5 are shown below in figure 6.

After correcting the offset of both original images, the difference rms dropped from 4.28 nm to 0.460 nm.

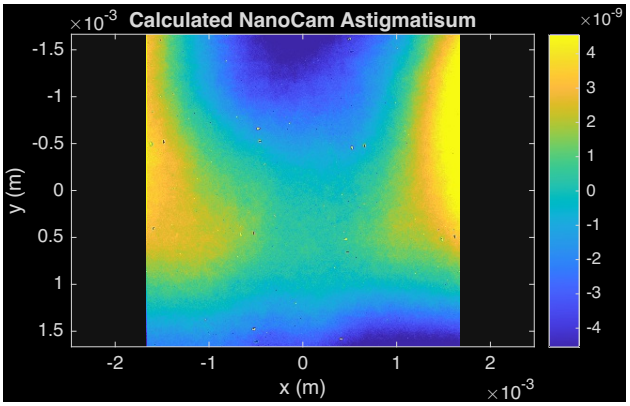

Figure 6: Offset from NanoCam. This is the offset I calculated using the described method from images 5a and 5b. Using this offset the difference between the images had an rms of 0.460 nm while before the difference had an rms of 4.28 nm.

4.2 Actuating on the Physical Mirror

4.2.1 Spoked End Mirror Imaging

The spoked end mirrors are made of a silicon substrate and have four protruding spokes, figure 3. I decided to image the uncoated spoked mirrors before attempting to bend them. This would allow us to check if the mount adds any stress to the mirrors. GQuEST is considering two types of spoked mirrors, an octagonal barrel mirror and a circular barrel mirror. The following images of the unmounted mirrors were created by stitching together a 3×3 grid of 3.5 mm $\times$ 4 mm images, utilizing the overlap to adjust the images.

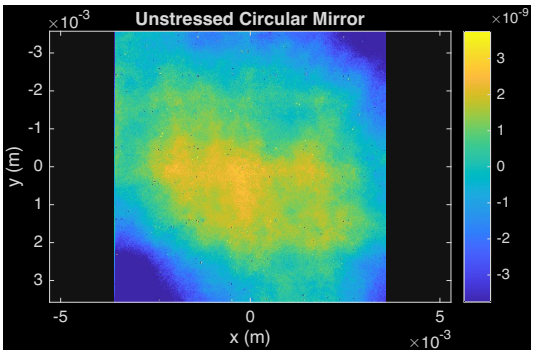

(a) Unmounted Circular Spoked Mirror

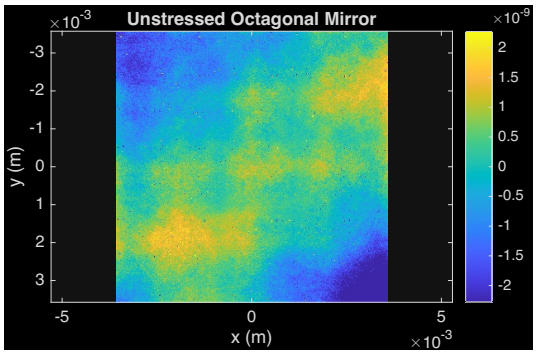

(b) Unmounted Octagonal Spoked Mirror

Figure 7: Unmounted Spoked Mirrors. In figure 7a, we can see the height map of the circular spoked mirror, weighted rms = 0.985 nm. In figure 7b, we can see the height map of the octagonal spoked mirror, weighted rms = 0.544 nm

.

The circular spoked mirror had a weighted rms of 0.985 nm while the octagonal spoked mirror had a weighted rms of 0.544 nm. The octagonal mirror appears to be initially flatter.

4.2.2 Flattening the Spoked End Mirrors

When securing the circular spoked mirror to the adjustable mount, the mirror surface appeared to stress and deform. We took this as an opportunity to test the adjustable mirror mount by flattening the mirror before the Bragg reflective coating was applied. By following the workflow described in figure 4 we were able to flatten the mirror by 2 orders of magnitude.

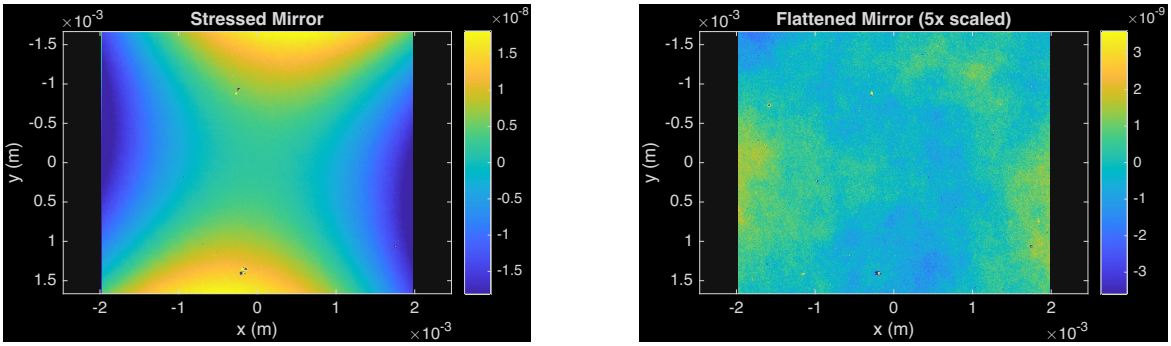

(a) Stressed Circular Mirror

(b) Flattened Circular Mirror

Figure 8: Flattening the Circular Spoked Mirror. The height map on the left is stressed mirror surface due to the securing the mirror to the adjustable mount. The height map on the right is the flattened mirror surface. Note the difference in scales: the stressed mirror is in 10s of nm, while the flattened mirror is in nm.

As shown in table 2, we reduced the rms of the mirror surface by roughly an order of magnitude, the focusing power of the quadratic terms by 2 orders of magnitude, and scattering due to residuals by an order of magnitude. And, most importantly, we reduced the total power loss of the mirror by 2 orders of magnitude. Additionally, the weighted rms of the unstressed circular mirror was 0.985 nm (63 ppm loss) and the weighted rms of the flattened mirror was 0.657 nm, indicating that the surface roughness of the mirror itself is contributing to how well we are able to flatten the mirror. Yet, it is crucial to note that the the vast majority of these deformations came from securing the mirror in the mount. Although the mount shows promise in correcting quadratic deformations, a better mounting system will need to be developed such that the flattened mirror achieves lower loss than the unmounted mirror.

Another interesting result of the mirror flattening is how much the calculated loss varies based on polynomial degree. As can be seen in figure 9, the total loss calculated can vary based on the max degree used in the least squares polynomial fit. One would expect that total loss would be constant across polynomial fit degree. We don't see this effect because the rms, key in calculating roughness loss, is only calculated on the very center of the mirror. Here the rms is lower as we are looking at the flattest part of quadratic deformations. This is clear in figure 10, as the rms on the limited domain is not an accurate measure of the rms of the entire mirror. Hence, the roughness loss is not a good figure of merit by itself. The HOM coupling, however, works with the extrapolated mirror map, and therefore takes into account the larger deformations. Only after removing these larger deformations can the rms be assumed to be constant across the mirror. This figure indicates that we are fitting out to a high enough degree to be accurate and that the majority of deformations left are

Circular and Octagonal Mirror Results						
	Circular Mirror			Octagonal Mirror		
	Original	Mounted	Flattened	Original	Mounted	Flattened
rms (m)	1.75×10^{-9}	9.07×10^{-9}	7.58×10^{-10}	9.89×10^{-10}	2.23×10^{-8}	9.53×10^{10}
weighted rms (m)	9.85×10^{-10}	7.73×10^{-9}	6.57×10^{-10}	5.44×10^{-10}	1.90×10^{-8}	8.30×10^{-10}
diopters	7.82×10^{-4}	3.014×10^{-2}	5.15×10^{-4}	4.64×10^{-4}	5.80×10^{-2}	1.20×10^{-3}
power scattered from residuals (ppm)	12	235	19	7.3	38.5	24.8
power lost into low order modes (ppm)	163	43,226	293	26.7	185,415	980
total loss (ppm)	175	43,461	312	34	185,453	1005

Table 2: Circular and Octagonal Mirror Results. This is a comparison of performance metrics for circular and octagonal mirrors in original, mounted, and flattened states.

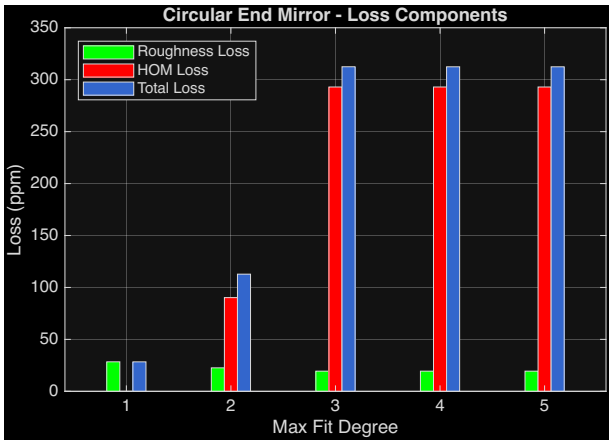

Figure 9: Total Loss as a Function of Polynomial Fit. As depicted in the graph, as the polynomial fit increases, the total loss appears to grow. This stabilizes after a 3rd degree fit, indicating we are fitting our mirror to an accurate depth.

cubic. These deformations don't lend themselves to the adjustable mirror mount, but might be able to be corrected using the other adjustment techniques.

Similar to the circular spoked mirror, the octagonal spoked mirror also exhibited some mounting stress. We also took the opportunity to flatten the octagonal mirror.

As can be seen in table 2 the octagonal mirror appeared to be more stressed initially than the circular mirror. However, we were still able to reduce the rms of the mirror to angstroms. The total loss of the mirror is also below the astigmatism of the NanoCam (roughly 5000ppm).

(a) Example of Complete Mirror Deformation

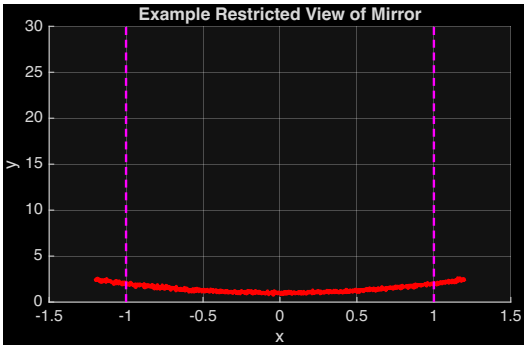

(b) Limited View of Mirror Deformation

Figure 10: Example Mirror Deformation. On the left hand side is a depiction of a parabolic 1D mirror deformation. On the right is a depiction of the limited domain the NanoCam is able to measure. It is clear that the rms measured on the limited domain cannot be said to be a constant across the mirror. It is necessary to first remove macroscopic deformations to measure surface roughness.

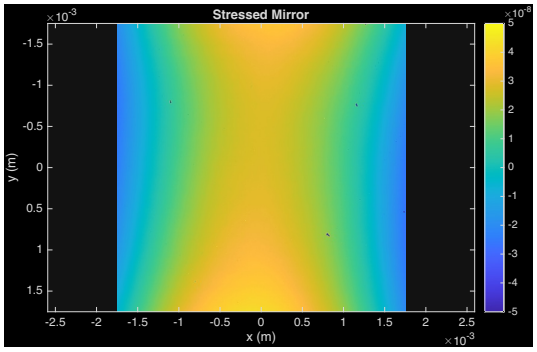

(a) Stressed Octagonal Mirror

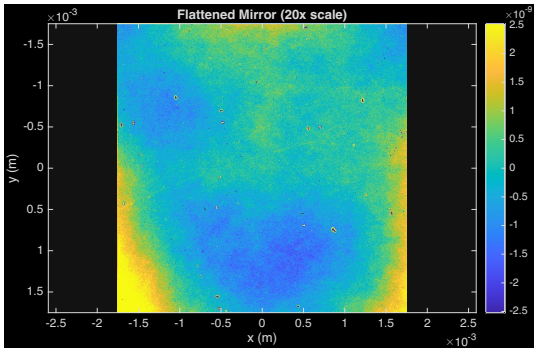

(b) Flattened Octagonal Mirror

Figure 11: Flattening the Octagonal Spoked Mirror. The height map on the left is stressed mirror surface due to the securing the mirror to the adjustable mount. The height map on the right is the flattened mirror surface. Note the difference in scales: the stressed mirror is in 10s of nm while the flattened mirror is in nm.

A key difference in the analysis of the circular and octagonal mirrors is how we corrected for the NanoCam astigmatism. The circular mirror used the original mirror as a reference, while the octagonal mirror used the calculated NanoCam astigmatism. This could be a reason we see such a difference in the total loss; however, both initial stress and flattening experience both could be leading causes.

4.2.3 Generating the +mode and Omode

As I have mentioned previously, we are tackling the +mode, Omode, and Xmode. Both initially stressed mirrors in figure 8a and figure 11a appear to be closest to the Xmode. To demonstrate that the mount is capable of correcting the +mode and Omode, I decided to induce these deformation on the octagonal spoked mirror, subtracting the reference stress

(figure 11a) to see the change in the mirror surface.

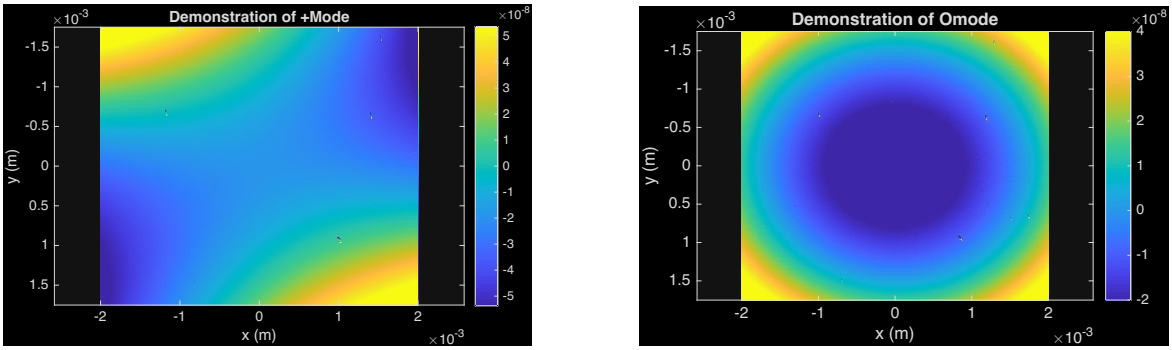

(a) Creating the +mode

(b) Creating the Omode

Figure 12: Demonstration of the +mode and Omode. This is a demonstration of generating the +mode and Omode. This was created by subtracting the stressed mirror from the final image, figure 11a.

As the reference stress appears to be primarily in the Xmode, being able to create clear +modes and Omodes demonstrates that we are able to create combinations of these quadratic corrections, which will be key for the final mirror.

+mode and Omode Creation		
	+mode	OMode
diopters	0.061	0.056
power coupled above $n + m = 2$	0.0455	0.0131
weighted rms of the mirror surface (m)	2.91×10^{-8}	1.82×10^{-8}
weighted rms of residuals of quadratic fit (m)	1.05×10^{-9}	7.59×10^{-10}

Table 3: Comparison between +mode and OMode. This table provides the accuracy and power of the +mode and OMode.

Because the weighted rms of the residuals from the quadratic fit is around an order of magnitude below the weighted rms of the original mirror surface, the vast majority of the deformation is quadratic. This indicates we are producing pure deformations. For reference, the focusing power of both modes is roughly 0.06 diopters, which is a third of what the PSAMS at LIGO are able to focus.

4.2.4 Repeatability Measurements

To test the repeatability of the mirror mount, I aimed to recreate the +mode that I constructed in figure 12a. Using the final image and rms value, I recreated the +mode twice. The statistics on all three mirrors can be seen in table 4.

The mirror appears to be relatively repeatable. Although the standard deviation of the total lensing power is two orders of magnitude below the mean, the focusing power into each mode

+mode Repeatability	
	Mean
Total lensing power (diopters)	$(6.33 \pm 0.05) \times 10^{-2}$
Lensing D_{20} (diopters)	$(2.4 \pm 0.5) \times 10^{-2}$
Lensing D_{11} (diopters)	$(4.5 \pm 0.3) \times 10^{-2}$
Lensing D_{02} (diopters)	$(3.7 \pm 0.5) \times 10^{-2}$

Table 4: Mirror Repeatability. This table shows the average and standard deviation of the +mode repeatability test. I attempted to recreate the initial +mode shown in figure 12a given 30 min, a picture of the original mirror, and the rms value. This table was constructed with three +modes.

appeared to vary more significantly. For the final implementation there will be less of a time requirement and we will be able to use focusing power data during the alignment. This should make the mirror adjustment more precise.

4.2.5 Mirror Drift

Finally, we were interested in how the mirror would drift over time. We started the mirror in a +mode and took lensing power data over the course of a week. As we expected the mirror relaxation rate to depend on the deformation amount, we chose to fit our data with an asymptotic exponential .

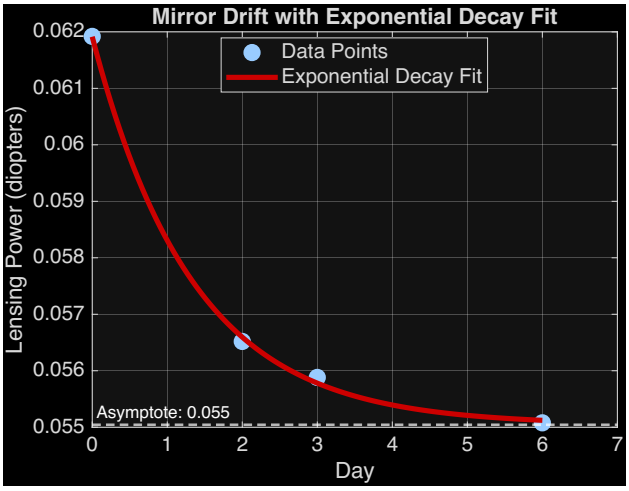

Figure 13: Mirror Drift. This is the total focusing power of the mirror as a function of time. We can see that after a week the power reduced roughly 10% but appears to stabilize.

From the graph (figure 13) we can see that the focusing power of the mirror appears to fit the trend line strongly (R-squared = .9994). The mirror appeared to lose about 10% of its focusing power over the course of a week, but then stabilize. I expect that this could be fixed by either re-stressing the mirror regularly in during the week or by overcompensating

the initial correction and anticipating the drift. Regardless of the final solution, the drift of the mirror does not seem overwhelmingly concerning for the limited data that we have.

5 Further Steps

The biggest next step for the GQuEST end mirrors is to apply the Bragg reflective coating. After this, we will be able to take more data on the coated mirrors, which will be the final mirrors in the GQuEST interferometer. Another important future improvement is controlling the stress the adjustable mount puts onto the mirror to make the flattening process easier. Some additional work should be done on finding the best NanoCam astigmatism correction, either calculating it from rotated images or by using a reference flat.

In summary, the mount corrected 3.0×10^{-2} diopters of focusing power with a precision of 2.6×10^{-4} diopters, reducing the total mirror loss from $43,461$ ppm to 312 ppm. Although the final goal for the mirror mount is to bring the loss below 50 ppm, the final GQuEST setup could also benefit from a couple of additional techniques to reduce the total loss. For the final interferometer, the end mirrors will have an anti-reflective coating of custom thickness applied to the back of the mirror in hopes to counteract some of the curvature. Furthermore, GQuEST plans to use matching pairs, hoping to have similar coupling into HOMs from both mirrors that will destructively interfere. Finally, there is a possibility to get the mirror surface polished which should reduce any loss due to surface roughness. This is expected to reduce the loss by an additional 2 orders of magnitude, meaning the adjustable mirror mount is getting the end mirrors to a reasonable loss level.

Acknowledgments

Thank you to Caltech, LIGO, NSF, Fermilab, the Department of Energy, and the Heising-Simons Foundation for making this opportunity possible. Thank you to Dr. Billingsley for her advice and for allowing us to use her 4D NanoCam HD (optical profiler) for our research. Finally, a special thanks to my mentors Daniel Grass and Dr. McCuller for all of their guidance, encouragement, and enthusiasm during this project.

References

[1]E. P. Verlinde and K. M. Zurek, "Observational signatures of quantum gravity in interferometers", Physics Letters B **822**, 136663 (2021).

[2]S. M. Vermeulen, T. Cullen, D. Grass, I. A. O. MacMillan, A. J. Ramirez, J. Wack, B. Korzh, V. S. H. Lee, K. M. Zurek, C. Stoughton, and L. McCuller, "Photon counting interferometry to detect geontropic space-time fluctuations with GQuEST", Physical Review X **15**, 011034 (2025).

[3]*Zernike polynomials*, in *Wikipedia*, Page Version ID: 1283251556 (Mar. 31, 2025).

[4]*Erin McGee 2024 SURF reports and presentation*, Foswiki, `https://wiki.mccullerlab.com/Main/ErinMcGee2024SURFReportsAndPresentation` (visited on 04/06/2025).

[5]R. A. Nyman and B. T. Walker, *Wave scattering from rough surfaces for good mirrors*, in , arXiv:2005.05201 [physics] (arXiv, May 2020).